Boronat Zaragoza, M.; López Auséns, JT.; Corma Canós, A. (2016). The acid-base and redox reactivity of CeO2 nanoparticles: Influence of the Hubbard U term in DFT plus U studies. Surface Science. 648:212-219. doi:10.1016/j.susc.2015.10.047

The acid-base and redox reactivity of CeO_2 nanoparticles. Influence of the Hubbard U term in DFT+U studies.

Mercedes Boronat, Tirso López-Ausens, Avelino Corma**

Instituto de Tecnología Química, Universidad Politécnica de Valencia – Consejo Superior de Investigaciones Científicas, Av .de los Naranjos, s/n, 46022 Valencia, Spain

*boronat@itq.upv.es, acorma@itq.upv.es.

Abstract

The interaction of small molecules with acid-base and redox centers in small $Ce_{21}O_{42}$ nanoparticles has been theoretically investigated using the DFT+U approach with the

PW91 functional and U=0,2 and 4 eV, in order to determine the influence of the U value on the trends observed in selected properties describing such interactions. CO adsorption at low coordinated Ce^{4+} Lewis acid centers, water adsorption and dissociation at acid-base pairs, formation of oxygen vacancy defects by removal of an oxygen atom from the system, and interaction of molecular O_2 with such defects have been considered. The largest effect of the value of U is found for the description of the reduced $Ce_{21}O_{41}$ nanoparticle. In all other cases involving stoichiometric and oxidized $Ce_{21}O_{42}$ and $Ce_{21}O_{43}$ systems, the trends in the calculated adsorption and reaction energies, optimized geometries, charge distribution and vibrational frequencies are quite similar at the three levels considered.

Keywords

Heterogeneous catalysis, DFT, ceria, nanoparticles, acid-base, redox

1. Introduction

Metal oxides are widely used in a large number of heterogeneously catalysed chemical processes of industrial interest, not only as support of metal nanoparticle catalysts, but

also as intrinsic catalysts. Among them, cerium oxide is widely used in the treatment of toxic emissions and exhaust gases from diesel engines, for removal of organics in wastewater, and as an electrolyte in solid oxide fuel cells. [1-3]

The catalytic activity of ceria is often related to its ability to undergo Ce^{4+}/Ce^{3+} redox cycles that facilitate formation and healing of oxygen vacancy defects, which are the active sites for a large number of reactions. [4] But in other cases this redox cycle does not participate in the reaction, and acid-base properties govern the catalytic activity of CeO_2. [5] For instance, it has been experimentally and theoretically demonstrated that water dissociation on reduced ceria surfaces does not require the Ce^{3+} cations present, but occurs at Ce^{4+} centers without involving any change in the oxidation state of cerium atoms. [6-9]

To gain insight into the catalytic performance of ceria at the molecular level, a large number of theoretical studies, often in close collaboration with experiments, have appeared in the literature in the last decade. [4, 10-20] However, the adequate theoretical description of the complicated electronic structure of CeO_2, and in particular of the Ce^{3+} cations present in the reduced material, is a challenging task. The main problem is related to the strongly correlated nature of the *4f* electrons, to the quasi degeneracy of different ionic configurations in which a highly localized *4f* electron state is occupied or empty, and to the lack of cancellation of the self-interaction error in DFT that leads to over delocalized electrons. Thus, in the case of reduced CeO_2, the two electrons left in the system when an oxygen atom is removed generating an oxygen vacancy defect (O_{vac}) should be localized on the *4f* states of the two Ce atoms close to the vacancy. But there exist many other metastable configurations very close in energy in which the two electrons are delocalized over some or all cerium atoms in the system,

and conventional DFT calculations may converge to any of these solutions, including the correct one which is in fact predicted to be the most stable. [21]

A simple and pragmatic approach to solve the problem is the so-called DFT+U approach, [22,23] which consists of correcting for on-site Coulomb correlation effects by adding a Hubbard-type U term to the Ce *4f* states. This way, the delocalized solutions are destabilized and calculations converge to the correct configuration with the two extra electrons localized on the two Ce atoms neighboring the vacancy. But the inclusion of a Hubbard U term in the DFT Hamiltonian makes it explicitly orbital dependent, which results in multiple self-consistent solutions corresponding to different orbital occupations. A major drawback of this approach is its non-universality, that is, the strong dependence of geometrical and electronic properties on the value of U. [10, 11, 24, 25, 26] In this sense, a recent study by Bennet and Jones has demonstrated that the adsorption energies of some small molecules over CeO_2(110) surface, as well as the thermodynamics of CO oxidation, do not follow a clear trend with the value of the Hubbard term for U values between 0 and 8.5 eV. [27] The choice of the U value is in many cases done by comparison of computed values of different properties with available experimental data. However, the U term is not a fitting parameter, but an intrinsic response property that measures the incorrect curvature of the conventional DFT energy as a function of orbital occupation, and should be determined in an internally consistent way. A self-consistent procedure based on a linear response approach has been proven to be an efficient way to determine the Hubbard U term for highly correlated transition and rare-earth metals [28, 29, 30, 31] In a different procedure, a U-ramping method that combines a slow increase of U with an iterative improvement of orbital occupations has been found able to converge to the ground state

solution among the multiple orbital-dependent solutions inherent to the DFT+U scheme in the cases of bulk UO_2, CoO and NiO, and a CeO_2(111) surface model. [32]

It is generally accepted in the literature that a U value between 4 and 6 eV is needed for a consistent description of the electronic structure of bulk CeO_2, including the band gap and the reduction energy of bulk CeO_2 to bulk Ce_2O_3, and it has been proposed that adding a U term also to the oxygen 2p electrons improves the description of such properties. [33] However, there is no guarantee that the optimum U value to describe bulk physical properties is also the correct choice to describe the reactivity of surfaces or of small CeO_2 nanoparticles. On the other hand, the catalytic activity of CeO_2 is not only associated to the generation of oxygen vacancy defects so that, in principle, the DFT+U scheme might not be necessary to describe properties of CeO_2 nanoparticles other than the stability of the reduced system. For this reason we explore in this contribution whether inclusion of a Hubbard U term in DFT calculations changes the theoretical description of the acid-base and redox properties of different sites present on CeO_2 nanoparticles of ~1 nm diameter. An enhanced catalytic activity has been reported for nanocrystalline CeO_2, composed of particles with diameter ≤ 5 nm. [5, 34-37] In the last years, Neyman et al. have investigated the electronic structure and reducibility of different $(CeO_2)_n$ and $(CeO_{2-x})_n$ with $n \leq 85$ nanoparticles as realistic models for nanocrystalline CeO_2 catalysts. [38-42] In their studies they have used the DFT+U approach with U=4 and the hybrid HSE06 functional when the system size allowed it, and have found a good correlation between the energies of formation of oxygen vacancy defects provided by both methods. We explore now the acid-base and redox reactivity of nanocrystalline CeO_2 by studying the interaction of CO, H_2O and O_2 molecules with several Lewis acid centers, acid-base pairs and oxygen vacancy defects, respectively,

present in the smallest $Ce_{21}O_{42}$ model described by Neyman et al., using a DFT+U approach with U=0, 2 and 4, the last value being the one used by Neyman et al.

2. Models and methods

All calculations in this work are based on periodic density functional theory (DFT) and were performed using the Perdew−Wang (PW91) exchange-correlation functional within the generalized gradient approach (GGA) [43, 44] as implemented in the Vienna Ab-initio Simulation Package (VASP) code. [45, 46] The valence density was expanded in a plane wave basis set with a kinetic energy cut off of 450 eV, and the effect of the core electrons in the valence density was taken into account by means of the projected augmented wave (PAW) formalism. [47] All calculations are spin polarized. Integration in the reciprocal space was carried out at the Γ k-point of the Brillouin zone. Charge distributions were estimated using the theory of atoms in molecules (AIM) of Bader using the algorithm developed by Henkelman. [48, 49] In the GGA+U approach a Hubbard U term is explicitly included in the calculations to improve the description of the localized Ce *4f* states. [22] The present GGA+U calculations were performed using the formalism of Dudarev et al. [50] with values of U = 0, 2 and 4.

Small CeO_2 nanoparticles were simulated by means of a $Ce_{21}O_{42}$ model system with a diameter of ~1 nm diameter, previously described by Migani et al. [40] This model contains two-coordinated O atoms at the edges between {100} and {111} facets, and three-coordinated O atoms in the {111} terraces, as well as Ce atoms in different coordination environments, as depicted in Figure 1. The $Ce_{21}O_{42}$ model was placed in a cubic box of 20x20x20 $Å^3$, large enough to avoid interactions between periodically repeated nanoparticles or adsorbates. During geometry minimizations, the positions of all atoms in the system were fully relaxed without any restriction, and vibrational frequencies were calculated numerically.

3. Results and discussion

3.1. Lewis acidity of low coordinated Ce^{4+} centres. Lewis acidity is related to the ability of the cationic M^{n+} centres in metal oxides to accept electron density from adsorbed molecules, and can be in principle described, among other parameters, by the net positive charge on the M^{n+} cations. Interaction of a Lewis acid site with a Lewis base molecule like CO causes a shift in the νCO vibrational frequency that is used to quantify the strength of this interaction, and therefore to provide a Lewis acidity scale. The adsorption of CO at the five different Ce^{4+} centres *a* to *e* shown in Figure 1 has been calculated at the DFT+U level using U = 0, 2 and 4. The optimized structures of CO adsorption complexes are depicted in Figure 2. The most relevant parameters providing information about this type of interaction are summarized in Table 1, and comparison of data obtained with different U values is done in Figure 3 and Figure S1 in the Supplementary Material.

Interaction energies E_{int} have been calculated as:

$$E_{int} = E(Ce_{21}O_{42}\text{--}CO)_{complex} - E(Ce_{21}O_{42}) - E(CO)$$

where $E(Ce_{21}O_{42}\text{--}CO)_{complex}$ is the total energy of the complex formed by adsorption of CO at the Ce^{4+} Lewis acid centres depicted in Figure 2, $E(Ce_{21}O_{42})$ is the total energy of the nanoparticle model, and E(CO) is the total energy of the CO molecule.

The net atomic charges on the five Ce^{4+} centres considered are quite similar, and differ by 0.07 e^- or less. CO interaction with these Lewis sites is weak. The molecule adsorbs on top of the Ce^{4+} cations at a distance of 2.9 – 3.0 Å, and the calculated E_{int} values are low, between -0.17 and -0.28 eV. The calculated νCO stretching frequencies are in all

cases shifted with respect to the gas phase value (2131 cm^{-1}) but there is not a clear correlation between the shift in the νCO frequency and the calculated adsorption energies.

The influence of the U value on the parameters studied is relatively small and quite systematic. The charge distribution, evaluated by the net charge on the Ce^{4+} cation, is the property for which the largest deviation between different U values is found (see Table 1 and Figure 3). The calculated qCe at each position increases by ~0.08 e^- as the U value changes from 0 to 4. Accordingly, with increasing U values, CO adsorption energies at each site become about -0.02 eV larger, and the optimized rCe-C distances become 0.02 Å shorter on average. The influence of the U parameter on the CO vibrational frequency is almost negligible, and νCO calculated values at each position differ by less than 3 cm^{-1}.

To facilitate comparison, the qCe, E_{int}, rCe-C and νCO values obtained with U=0 and U=2 are plotted against the same values obtained with the reference U=4 value in Figure S1, and the correlation coefficients of the regression lines obtained are shown beside the lines. The largest deviation between different U values is found for the net charge on the Ce^{4+} cation, with a correlation coefficient for U=0 of only 0.92. All other properties investigated are similarly described at all theoretical levels.

3.2. Acid-base pairs. Interaction with water. Water is also a Lewis base whose electrons in the lone pair on O can interact with the cationic M^{n+} centres in metal oxides. It also possesses two H atoms that can form strong hydrogen bonds with the basic O atoms of the metal oxide surface. Both interactions can eventually lead to dissociation of one O-H bond in the water molecule and formation of two hydroxyl groups on the oxide surface. The adsorption and dissociation of water at three different

sites on a $Ce_{21}O_{42}$ nanoparticle has been now investigated using DFT+U with U=0, 2 and 4. The acid base pairs formed by Ce at positions *a*, *b* and *c* combined with O atoms labelled A, B and C, respectively, have been considered. The optimized structures of water adsorbed at Ce^{4+} centres and of the hydroxylated systems resulting from O-H bond breaking are depicted in Figure 4. Adsorption E_{ads} and reaction ΔE energies, together with selected optimized distances and calculated vibrational frequencies are summarized in Table 2, and comparison of data obtained with different U values is done in Figure 5 and Figure S2 in the Supplementary Material. Adsorption energies E_{ads} have been calculated as:

$$E_{ads} = E(Ce_{21}O_{42}\text{--}H_2O)_{complex} - E(Ce_{21}O_{42}) - E(H_2O)$$

where $E(Ce_{21}O_{42}\text{--}H_2O)_{complex}$ is the total energy of the complex formed by adsorption of H_2O at the acid-base pairs depicted in Figure 4, $E(Ce_{21}O_{42})$ is the total energy of the nanoparticle model, and $E(H_2O)$ is the total energy of the H_2O molecule. Reaction energies have been calculated as:

$$\Delta E = E(Ce_{21}O_{42}\text{--H-OH})_{system} - E(Ce_{21}O_{42}\text{--}H_2O)_{complex}$$

where $E(Ce_{21}O_{42}\text{--H-OH})_{system}$ is the total energy of the hydroxylated systems resulting from O-H bond dissociation.

As shown in Figure 4, the oxygen atom of water (Ow) interacts with the Ce^{4+} Lewis acid centres at the three positions considered, and an additional hydrogen bond between a proton of water and an oxygen atom of the ceria surface (Os) is formed at *b*B and *c*C sites. This is clearly reflected in the optimized values of the rOs-H distance, that is 1.7 and 1.8 Å at *b*B and *c*C sites, respectively, and significantly larger, close to 3.0 Å at aA

position. However, the calculated adsorption energy of water at *a*A site is only ~0.1 eV lower than at the other two positions, suggesting a very strong Lewis acid-base interaction at this position. Dissociation of one of the two O-H bonds in water produces a hydroxyl fragment that remains attached to the Ce^{4+} cation, and a proton that is transferred to an oxygen atom. This process is always exothermic, but the calculated reaction energy at *a*A site is much larger than at the other two positions. The reason is that water dissociation at *b*B and *c*C sites also involves the rupture of the stabilizing hydrogen bonds between the water proton and oxygens B and C, with the corresponding energy cost. The breaking of the O-H bond in adsorbed water results in formation of two different types of hydroxyl groups: a monocoordinated OH_a group consisting of the deprotonated water fragment attached to the Ce^{4+} cation, and a bridge OH_b group arising from protonation of a surface Os atom. These two types of hydroxyl group are formed at the three positions considered, and their stretching vibrational frequencies are clearly different, larger than 3800 cm^{-1} for νOH_a and around 3770-3780 cm^{-1} for νOH_b.

This picture is not affected by the value of the U parameter used in the calculations. The same optimized structures and the same relative stability between them is found at all theoretical levels. Calculated adsorption and reaction energies systematically increase with increasing the U value, with the difference between the values obtained using U=0 and U=4 being less than 0.05 eV for E_{ads} and 0.12 eV at most for ΔE. A clearly linear relationship with an excellent correlation is found for both energies (see Figure S2 in the Suplementary Material). The optimized rCe-Ow distances become systematically shorter as the U value increases, but this trend is not always observed for the rOs-H bond lengths. On the other hand, the calculated νOH vibrational frequencies always increase with increasing the U value, but the linearity of the correlations are not excellent.

A recent study of water adsorption and dissociation over a CeO_2(111) surface using several approximations to exchange and correlation within DFT, namely GGA, GGA+U, hybrid functional and van der Waals functional, concluded that all methods predict similar structures and energetics, in line with our present results.[8]

3.3. Redox properties. The most important and of widespread use catalytic applications of CeO_2 are based on its redox properties, in particular on its ability to change oxidation state from Ce^{4+} to Ce^{3+}. Removal of an oxygen atom from the CeO_2 surface leaving two electrons on the solid creates an oxygen vacancy defect (O_{vac}) and the reduction of two Ce^{4+} cations to Ce^{3+}. These oxygen vacancy defects can be healed by molecular O_2 generating peroxide and superoxide species, responsible for the redox catalytic activity of CeO_2. [12, 13, 35, 51, 52]

We have now studied the adsorption of molecular O_2 at Ce^{4+} centres *b* and *c* on the stoichiometric $Ce_{21}O_{42}$ nanoparticle, as well as the formation of reduced $Ce_{21}O_{41}$ systems by removal of oxygen atoms at positions A, B, and C in stoichiometric $Ce_{21}O_{42}$, and the formation of oxidized $Ce_{21}O_{43}$ systems by addition of oxygen atoms at positions *a, b* and *c* on the stoichiometric $Ce_{21}O_{42}$ nanoparticle. In this last case, the resulting systems are equivalent to those obtained by adsorption of molecular O_2 at the three oxygen vacancy defects A, B and C present in the reduced $Ce_{21}O_{41}$ models, so that they have been labelled as A, B and C in Figures 6 and 7 and in Table 3.

The interaction energies E_{int} at sites *b* and *c* on stoichiometric $Ce_{21}O_{42}$ are calculated as:

$$E_{int} = E(Ce_{21}O_{42}\text{--}O_2)_{complex} - E(Ce_{21}O_{42}) - E(O_2)$$

where $E(Ce_{21}O_{42}\text{--}O_2)_{complex}$ is the total energy of the complex formed by adsorption of O_2 at the Ce^{4+} Lewis acid centres depicted in Figure 6, $E(Ce_{21}O_{41})$ is the total energy of the $Ce_{21}O_{42}$ model, and $E(O_2)$ is the total energy of an isolated O_2 molecule in its triplet state. The energy of formation of oxygen vacancy defects E_{Ovac} is calculated as:

$$E_{Ovac} = E(Ce_{21}O_{41}) + 1/2\ E(O_2) - E(Ce_{21}O_{42})$$

where $E(Ce_{21}O_{41})$ and $E(Ce_{21}O_{42})$ are the total energies of the $Ce_{21}O_{41}$ and $Ce_{21}O_{42}$ models, respectively, and $E(O_2)$ is the total energy of an isolated O_2 molecule in its triplet state. A more realistic pathway for the reduction of $Ce_{21}O_{42}$ nanoparticles is their reaction with H_2 generating H_2O and a reduced $Ce_{21}O_{41}$ system. The reduction energy E_{red} is calculated as:

$$E_{red} = E(Ce_{21}O_{41}) + E(H_2O) - E(Ce_{21}O_{42}) - E(H_2)$$

where $E(Ce_{21}O_{41})$ and $E(Ce_{21}O_{42})$ are the total energies of the $Ce_{21}O_{41}$ and $Ce_{21}O_{42}$ models, respectively, and $E(H_2O)$ and $E(H_2)$ are the total energies of isolated H_2 and water molecules. On the other hand, the energies of formation of oxidized $Ce_{21}O_{43}$ systems E_{int} have been calculated in two ways, either related to the stoichiometric model:

$$E_{int} = E(Ce_{21}O_{43}) - E(Ce_{21}O_{42}) - 1/2\ E(O_2)$$

or to the reduced system:

$$E_{int} = E(Ce_{21}O_{43}) - E(Ce_{21}O_{41}) - E(O_2)$$

where $E(Ce_{21}O_{43})$ is the total energy of the oxidized models depicted in Figure 6.

The interaction of molecular O_2 with stoichiometric $Ce_{21}O_{42}$ nanoparticles is weak, with calculated interaction energies lower than -0.1 eV. In the optimized structures *b* and *c* depicted in Figure 6, the O_2 molecule is at a distance larger than 3.0 Å from the Ce^{4+} cations. The charge transferred to O_2 is almost negligible, less than -0.015 e-, and as a consequence the O-O is not altered and the calculated νOO vibrational frequencies are not too different from the gas phase value obtained at the same theoretical level, which is 1565 cm^{-1}. No relevant differences between the data obtained with increasing values of the U parameter are observed in Table 3 and Figure 7 for structures *b* and *c*. The interaction energies differ by less than 0.01 eV, the charge transferred by less than 0.006 e-, the optimized O-O bond lengths are equivalent, and the largest deviation in the calculated νOO vibrational frequencies is 5 cm^{-1}.

A completely different picture is found for the adsorption of an oxygen atom on the stoichiometric $Ce_{21}O_{42}$ model resulting in formation of structures A, B and C in Figure 6. In all cases, the extra oxygen atom binds to a bi-coordinated oxygen atom present at the particle surface forming a covalent peroxide species, similar to that previously described for atomic oxygen adsorption on CeO_2 surfaces. [12,13] The two oxygen atoms in each of these structures are directly attached to Ce^{4+} cations, the optimized O-O bond lengths increase to values larger than 1.4 Å, and as a consequence the vibrational frequencies shift to significantly lower values, between 650 and 900 cm^{-1} depending on the adsorption site. The reason for these changes is the large negative charge transferred to O_2, between -1.1 and -1.6 e^- depending on the site of adsorption. If we consider this process as the adsorption of molecular O_2 at an oxygen vacancy defect, what happens is that the extra e- located in the reduced Ce^{3+} cations close to the vacancy are transferred to the anti-bonding π* MO of O_2, resulting a O-O bond weakening and a concomitant increase in the O-O bond length.

With regard to the influence of the U value, analysis of the data summarized in Table 3 and the plots in Figure 7 show an increase of up to -0.07 e- in the net atomic charge transferred to O_2 as U changes from U=0 to U=4. As a consequence, the optimized O-O distances differ by 0.007 Å on sites B and C, and as much as 0.051 Å on site C. This produces a shift in the calculated vibrational frequencies of 9-14 cm^{-1} when U increases from U=0 to U=4. It should be noted that despite these differences in the computed values of selected properties, the trends obtained as a function of the site on the nanoparticle are the same for all values of U.

The interaction energies calculated with respect to the stoichiometric $Ce_{21}O_{42}$ system (values in parenthesis in Table 3) are almost negligible, even slightly endothermic at some sites, and vary by less than 0.03 eV as a function of the value of the U parameter.

However, when these interaction energies are calculated with respect to the reduced $Ce_{21}O_{41}$ system, the E_{int} values are considerably larger, of the order of -2, -3 eV, and differ by 0.8 eV depending on the value of U. Table 3 shows that the energy required to remove an oxygen atom from stoichiometric $Ce_{21}O_{42}$ generating an oxygen vacancy defect using U=0 is systematically larger by 0.8 eV than that obtained using U=4. The order of stability of the oxygen vacancy defects C > B > A is the same at both computational levels, and the most favorable position to remove an oxygen atom is site C, in agreement with previous work. [40] The energy of formation of an oxygen vacancy defect E_{Ovac} at site C is 2.65 eV with U=0 and 1.71 eV with U=4. This last value is equivalent to that obtained by Migani et al. at the same theoretical level, 1.67 eV, but too low compared with the 2.05 eV obtained using the hybrid HSE06 xc functional.[40] Finally, the reduction energies E_{red} calculated for the reaction of $Ce_{21}O_{42}$ with H_2 generating a $Ce_{21}O_{41}$ system and H_2O follow the same trends as the energies of formation of oxygen vacancy defects E_{Ovac} , that is, site C is more reducible than B and

A. However, the calculated E_{red} values are positive when U=0, indicating an endothermic process, and negative, that is, exothermic, when U=4. It is therefore at this point where the problems associated to the strongly correlated nature of the *4f* electrons and to the lack of cancellation of the self-interaction error in conventional DFT are made apparent, and relevant differences between the relative stability of reduced $Ce_{21}O_{41}$ and stoichiometric $Ce_{21}O_{42}$ systems are found as a function of the value of the Hubbard U parameter.

4. Conclusions

The interaction of CO with Lewis acid centers, the adsorption and dissociation of H_2O at acid-base pairs, and the adsorption of molecular O_2 at Ce^{4+} centres and oxygen vacancy defects present in CeO_2 nanoparticle models of ~1 nm diameter have been theoretically investigated using the DFT+U approach with U=0, 2 and 4 eV. Analysis of the data obtained at the three computational levels considered leads to the following general conclusions: CO interaction with low-coordinated Ce^{4+} centers is weak, and produces a shift in the νCO calculated vibrational frequencies ranging from of 13 to 44 cm^{-1} depending on the position of the Ce^{4+} cation. Water forms Lewis acid-base adducts by interaction of the water oxygen atom with the Ce^{4+} cation, and in some cases an additional hydrogen bond between a water proton and a basic oxygen atom of ceria is also formed. Dissociation of water at these acid-base pairs is always exothermic and generates two types of hydroxyl groups. Oxygen vacancy defects can be created on the ceria nanoparticles by removal of a surface oxygen atom, with the most stable defect being generated by removal of a bicoordinated oxygen atom at the edge between (100) and (111) facets, in agreement with previous work. The same site is the most reactive in the reduction of CeO_2 nanoparticles with H_2 generating water. Interaction of O_2 with

stoichiometric CeO_2 nanoparticles is weak, but its adsorption at the oxygen vacancy defects is highly exothermic and results in formation of stable superoxide species, experimentally observed by IR spectroscopy. All these conclusions are general, and do not change as a function of the value of the U parameter used in the calculations.

Comparison of the results obtained with U=0, 2 and 4 indicates that inclusion of a Hubbard U parameter in the calculations produces small changes in the optimized bond lengths ($\leq$ 0.05 Å, ~1-2%) and vibrational frequencies (from 0 to 23 cm^{-1}, which is less than 1% except in one case which is 2%), and slightly larger differences in the net atomic charges (< 0.1 e-, ~4%) The influence of the U parameter is more relevant in the case of adsorption and reaction energies associated to acid-base interactions, that can be increased by 10-15% when comparing the values obtained with U=0 and U=4. But the major influence of the U value is found in the stability of the reduced nanoparticles; in this case the energy of formation of a oxygen vacancy defect decreases by ~ 0.8 eV when the value of U increases from 0 to 4 eV. However, once the oxygen vacancy defecs are healed by O_2 molecules, the resulting peroxide species are similarly described by the three computational levels considered. These conclusions might be helpful to guide the choice of the computational level required to perform theoretical studies of reaction mechanisms catalyzed by ceria nanoparticles.

Acknowledgements

Financial support from the Spanish Science and Innovation Ministry (Consolider Ingenio 2010-MULTICAT CSD2009-00050 and Subprograma de apoyo a Centros y Universidades de Excelencia Severo Ochoa SEV 2012 0267) is acknowledged. Red Española de Supercomputación (RES) and Centre de Càlcul de la Universitat de València are gratefully acknowledged for computational facilities and technical

assistance. T. L.-A. thanks ITQ for a contract. We thank Konstantin Neyman for providing the $Ce_{21}O_{42}$ nanoparticle model.

Table 1. Calculated values at the DFT+U level with U=0, 2, 4 of some relevant parameters related to Lewis acidity of Ce^{4+} centers. Net atomic charge on Ce (qCe, in e^-), interaction energy with CO (E_{int}, in eV), optimized Ce-C distance in the adsorption complex (rCe-C, in Å), and C-O vibrational frequency (νCO, in cm^{-1}).

	U	*a*	*b*	*c*	*d*	*e*
qCe (e^-)	0	2.16	2.18	2.21	2.20	2.23
	2	2.21	2.21	2.24	2.25	2.27
	4	2.24	2.25	2.28	2.29	2.31
E_{int} (eV)	0	-0.22	-0.25	-0.26	-0.20	-0.17
	2	-0.23	-0.26	-0.27	-0.21	-0.17
	4	-0.24	-0.27	-0.28	-0.22	-0.17
rCe-C (Å)	0	3.039	2.937	2.907	3.007	2.962
	2	3.027	2.935	2.895	2.999	2.943
	4	3.022	2.931	2.885	2993	2.936
νCO (cm^{-1})	0	2175	2150	2152	2168	2155
	2	2175	2148	2151	2169	2155
	4	2175	2147	2150	2169	2155

Table 2. Calculated values at the DFT+U level with U=0, 2, 4 of some relevant parameters describing the interaction of water with acid-base pairs on $Ce_{21}O_{42}$ nanoparticle. Adsorption and reaction energies (E_{ads}, and ΔE, in eV), optimized Ce-Ow and Os-H distances in the adsorption complex (rCe-Ow and rOs-H, in Å), and O-H vibrational frequencies (νOH_a and νOH_b, in cm^{-1}).

	U	*a*A	*b*B	*c*C
E_{ads} (eV)	0	-0.56	-0.69	-0.66
	2	-0.58	-0.71	-0.68
	4	-0.61	-0.74	-0.70
rCe-Ow (Å)	0	2.655	2.642	2.656
	2	2.645	2.633	2.646
	4	2.634	2.620	2.638
rOs-H (Å)	0	3.002	1.718	1.833
	2	2.968	1.729	1.850
	4	2.948	1.721	1.805
ΔE (eV)	0	-1.02	-0.30	-0.14
	2	-1.08	-0.34	-0.17
	4	-1.14	-0.34	-0.20
νOH_a (cm^{-1})	0	3809	3804	3808
	2	3819	3811	3814
	4	3827	3827	3821
νOH_b (cm^{-1})	0	3768	3773	3776
	2	3772	3775	3776
	4	3775	3788	3781

Table 3. Calculated values at the DFT+U level with U=0, 2, 4 of some relevant parameters describing oxygen vacancy defects, the interaction of molecular O_2 with Ce^{4+} sites on stoichiometric $Ce_{21}O_{42}$ nanoparticle and with oxygen vacancy defects on the reduced $Ce_{21}O_{41}$ system, and the reduction of $Ce_{21}O_{42}$ nanoparticles with H_2. Interaction energies (E_{int}, in eV) [a], net charge on O_2 (qO_2, in e^-), optimized O-O bond lengths (rOO, in Å), O-O vibrational frequencies (νOO, in cm^{-1}), energies of formation of defect (E_{Ovac}, in eV) and of reduction with H_2 (E_{red}, in eV).

	U	*b*	*c*	A	B	C
E_{int} (eV) [a]	0	-0.08	-0.07	3.18 (0.06)	-2.88 (-0.05)	-2.50 (0.15)
	2	-0.09	-0.07	(0.07)	(-0.06)	(0.16)
	4	-0.09	-0.07	-2.43 (0.07)	-2.10 (-0.08)	-1.54 (0.17)
qO_2 (e-)	0	-0.012	-0.009	-1.100	-1.113	-1.523
	2	-0.014	-0.011	-1.125	-1.135	-1.555
	4	-0.015	-0.012	-1.169	-1.155	-1.589
rOO (Å)	0	1.233	1.235	1.427	1.453	1.409
	2	1.233	1.235	1.432	1.456	1.415
	4	1.233	1.235	1.478	1.460	1.411
νOO (cm^{-1})	0	1561	1551	917	900	677
	2	1560	1548	911	896	670
	4	1559	1546	904	891	663
E_{Ovac} (eV)	0			3.24	2.83	2.65
	4			2.50	2.02	1.71
E_{red} (eV)	0			0.65	0.24	0.06
	4			-0.09	-0.57	-0.88

[a]Interaction energies E_{int} have been calculated with respect to reduced $Ce_{21}O_{41}$ system as $E_{int} = E(Ce_{21}O_{43}) - E(Ce_{21}O_{41}) - E(O_2)$. The values in parenthesis correspond to E_{int} calculated with respect to to stoichiometric $Ce_{21}O_{42}$ system as $E_{int} = E(Ce_{21}O_{43}) - E(Ce_{21}O_{42}) - 1/2\ E(O_2)$.

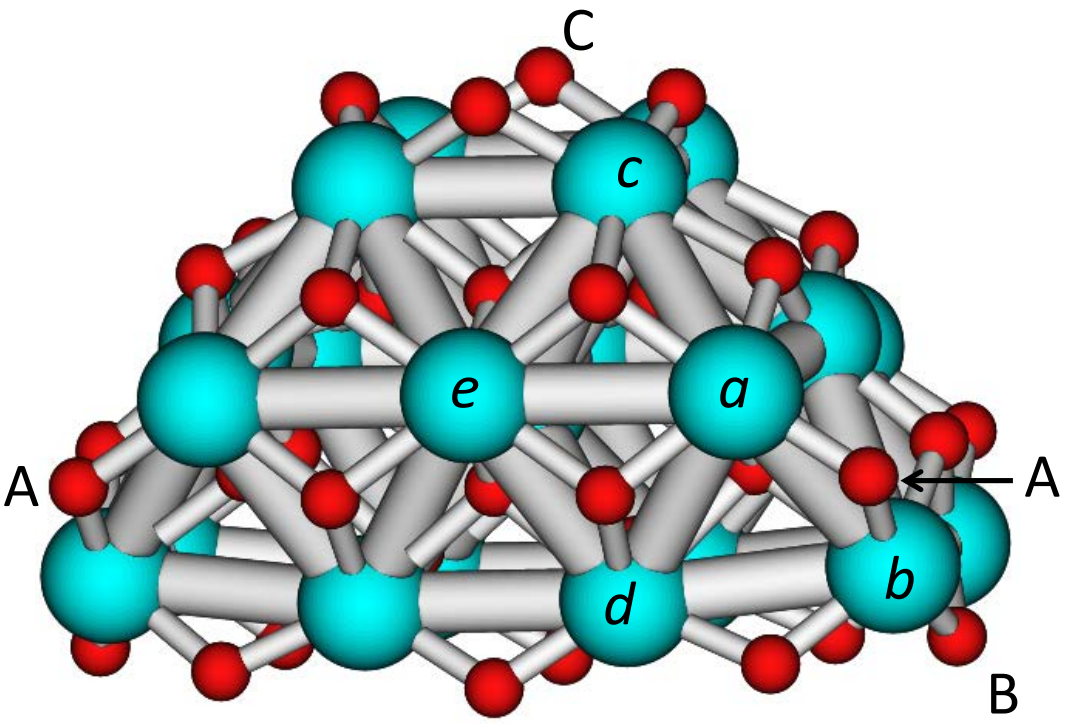

Figure 1. $Ce_{21}O_{42}$ nanoparticle model with the labeling of Ce atoms (italic letters) and O atoms (capital letters) studied.

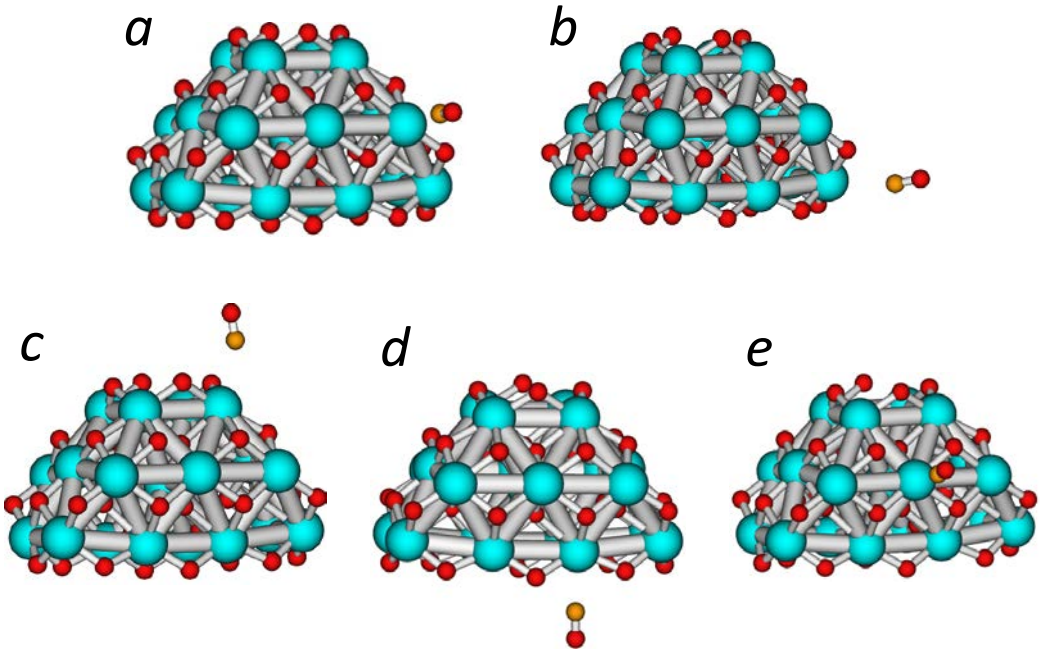

Figure 2. Optimized structures of CO adsorbed at different Ce^{4+} Lewis acid centres.

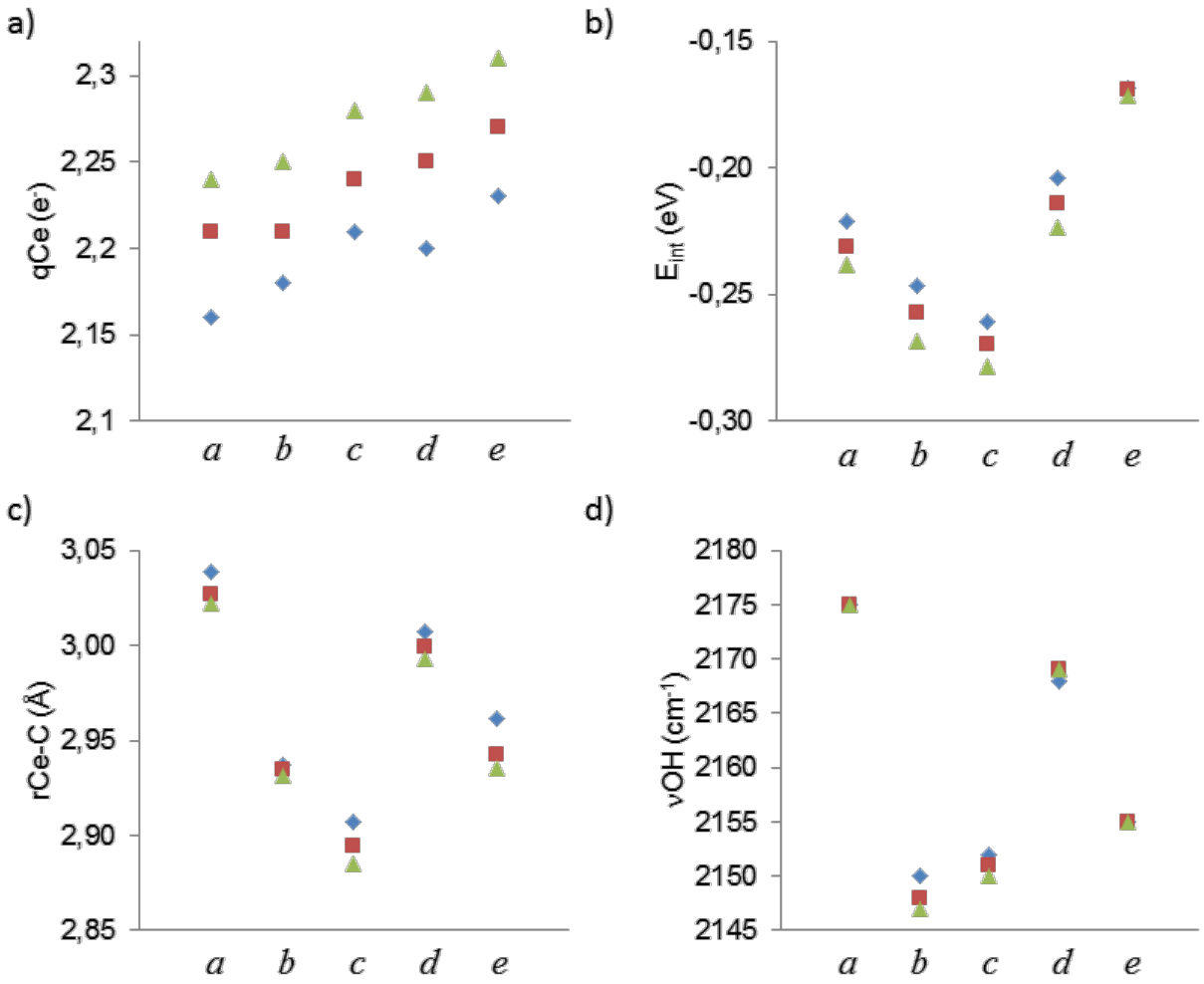

Figure 3. Values of a) net charge on Ce^{4+} Lewis centres (q_{Ce}) b) interaction energy of CO (E_{int}) c) optimized Ce-C distances (r_{Ce-CO}) and d) C-O vibrational frequency (ν_{CO}) calculated at DFT+U level with U=0 (blue rhombus), U=2 (red squares) and U=4 (green triangles) for CO adsorbed at the different Ce^{4+} Lewis acid centres *a* to *e* depicted in Figure 2.

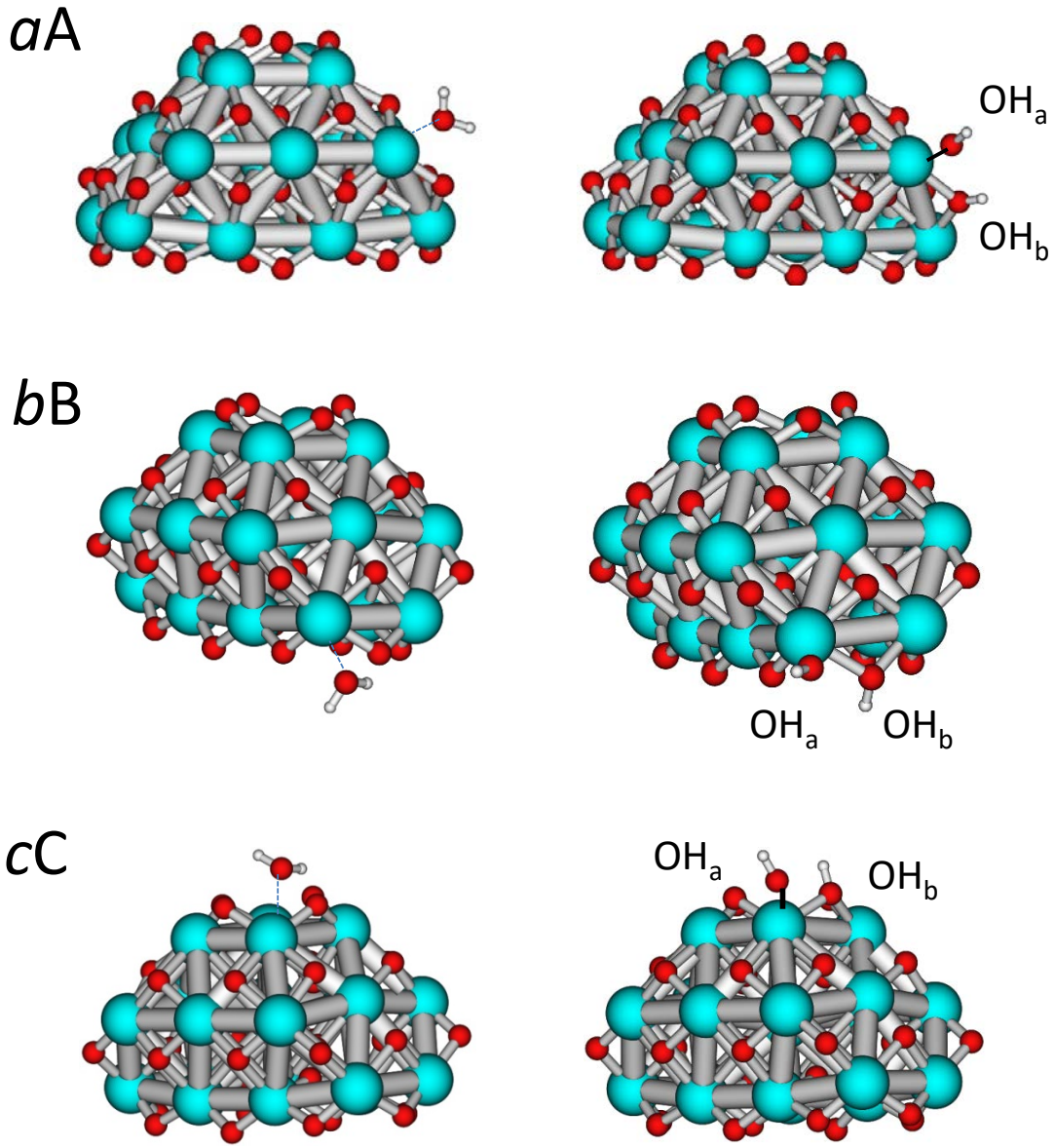

Figure 4. Optimized structures of H_2O adsorbed (left) and after dissociation of an O-H bond (right) at different acid-base pairs on stoichiometric $Ce_{21}O_{42}$ nanoparticle.

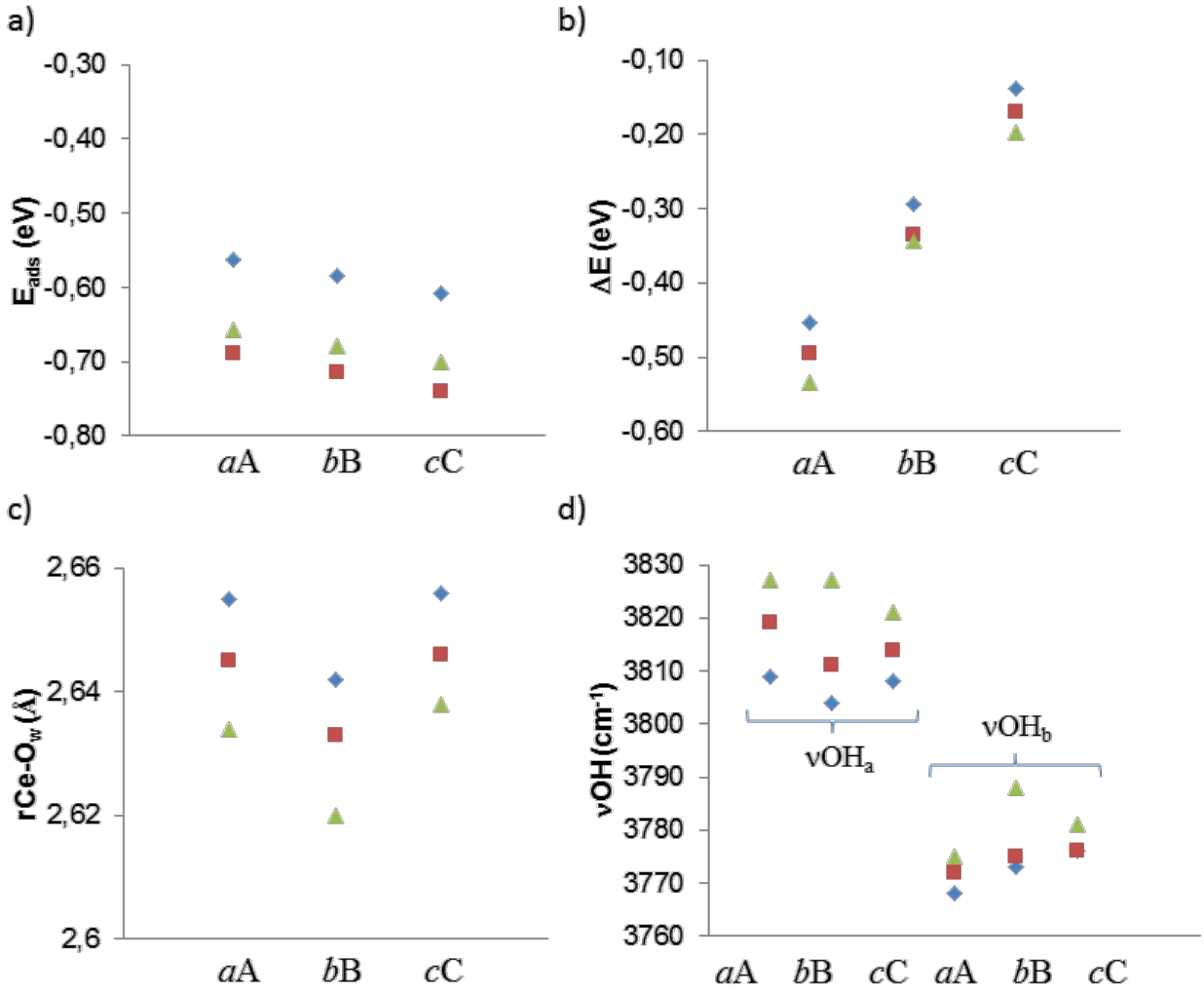

Figure 5. Values of a) water adsorption energy (E_{ads}) b) reaction energy for water dissociation (ΔE) c) optimized Ce-O distances ($r_{Ce\text{-}Ow}$) and d) O-H vibrational frequencies (ν_{OH}) calculated at DFT+U level with U=0 (blue rhombus), U=2 (red squares) and U=4 (green triangles) for H_2O interacting with different acid-base pairs on stoichiometric $Ce_{21}O_{42}$ nanoparticle as depicted in Figure 4.

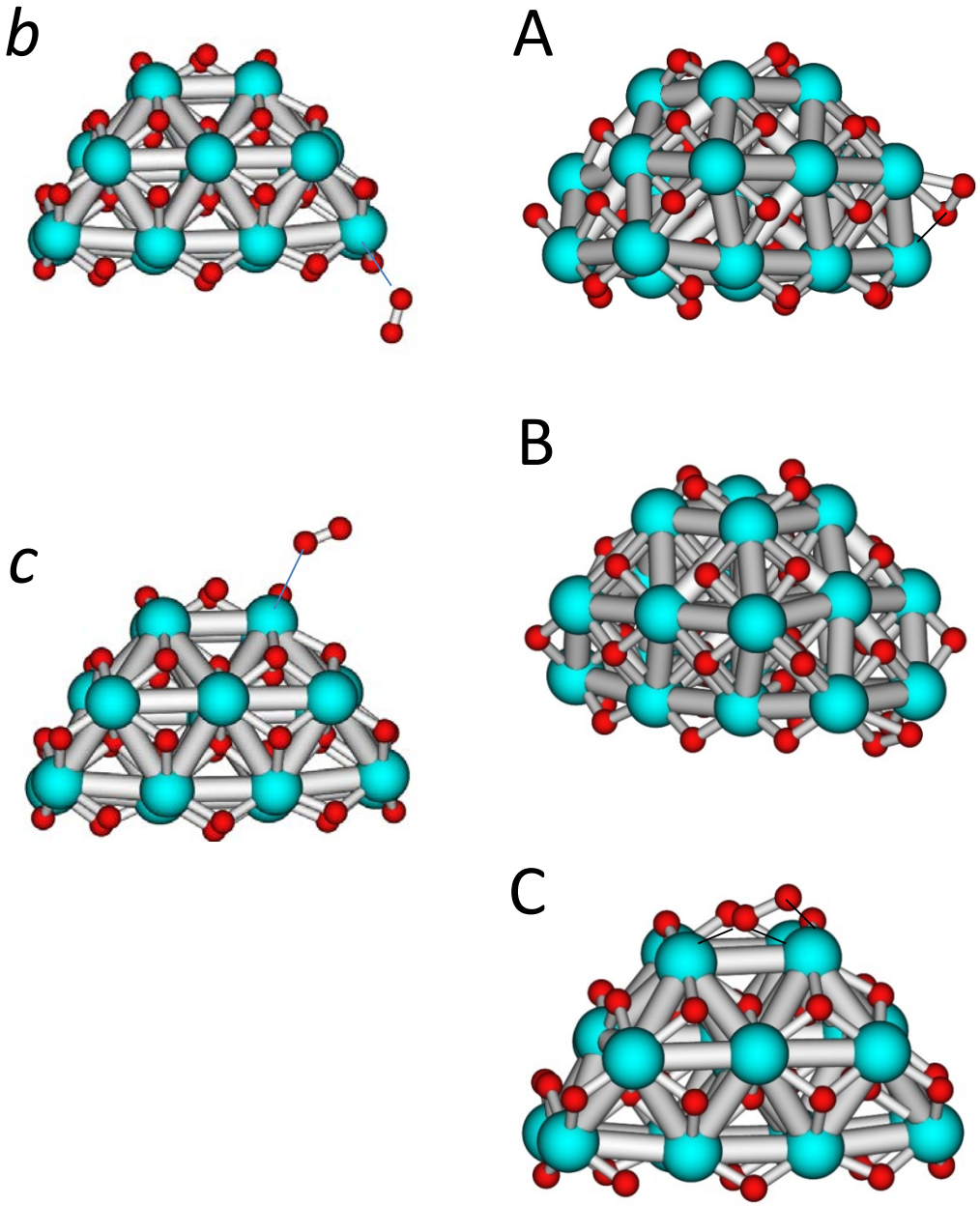

Figure 6. Optimized structures of O_2 adsorbed at *a* and *b* Ce^{4+} centres on stoichiometric $Ce_{21}O_{42}$ nanoparticle, and at A, B and C oxygen vacancy defects present in reduced $Ce_{21}O_{41}$ model forming the corresponding $Ce_{21}O_{43}$ oxidized systems.

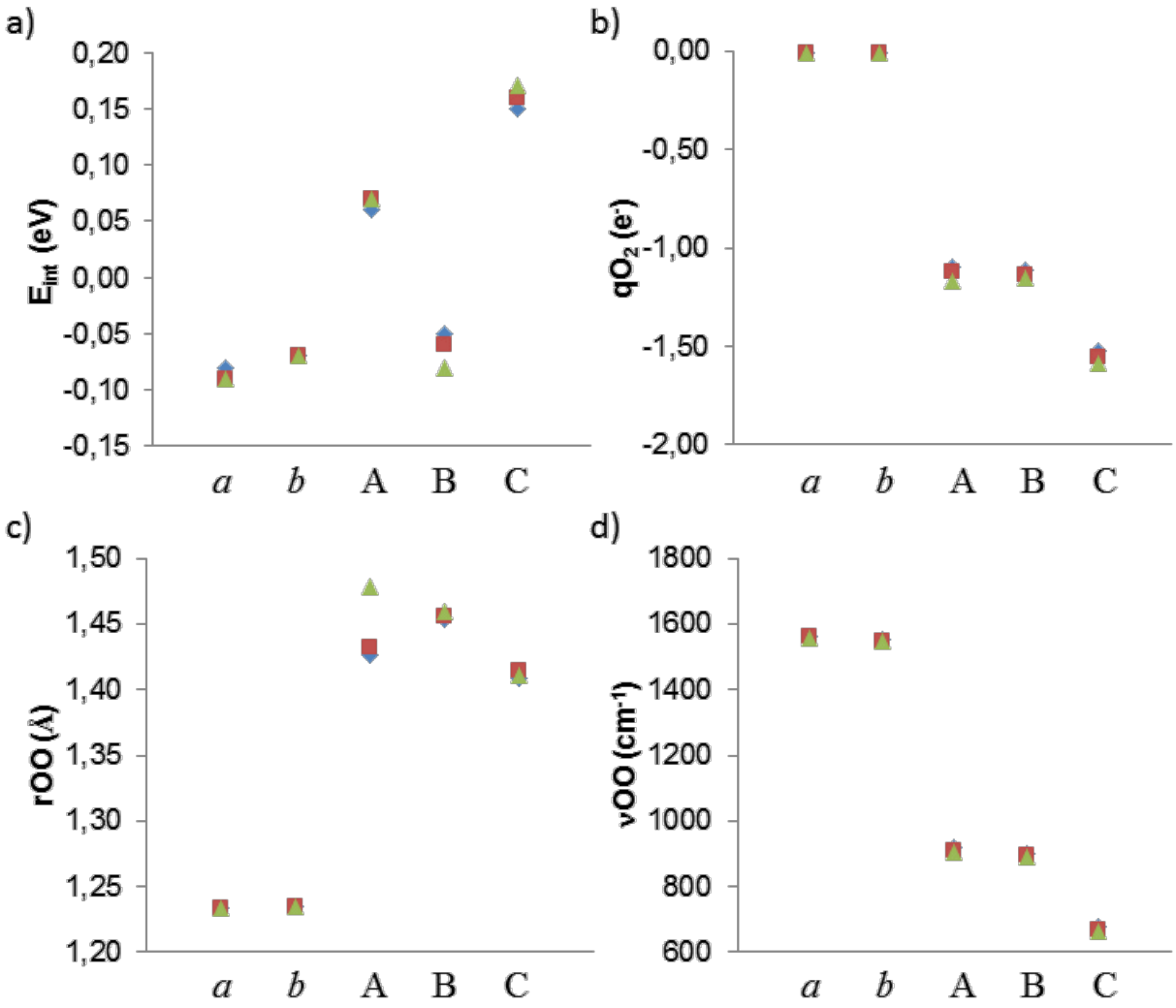

Figure 7. Values of a) O_2 interaction energy (E_{int}) b) net charge on O_2 molecule (qO_2) c) optimized O-O distances (r_{OO}) and d) O-O vibrational frequencies (ν_{OO}) calculated at DFT+U level with with U=0 (blue rhombus), U=2 (red squares) and U=4 (green triangles) for O_2 adsorbed at the *a* and *b* Ce^{4+} centres and the A, B and C oxygen vacancy defects depicted in Figure 6.

References

[1] A. Trovarelli, P. Fornasiero, Eds. Catalysis by Ceria and Related Materials; Imperial College Press, London, UK, (2002).

[2] R. Gorte, *AIChE J.* 56 (2010) 1126.

[3] L. Vivier, D. Duprez, *ChemSusChem* 3 (2010) 654.

[4] J. Paier, C. Penschke, J. Sauer, *Chem. Rev.* 113 (2013) 3949.

[5] S. Laursen, D. Combita, A. B. Hungria, M. Boronat, A. Corma, *Angew. Chem. Int. Ed.* 17 (2012) 4190.

[6] M. A. Henderson, C. Perkins, M. H. Engelhard, S. Thevuthasan, C. H. Peden, Surf. Sci. 526 (2003) 1.

[7] M. Fronzi, S. Piccinin, B. Delley, E. Traversa C. Stampfl, Phys. Chem. Chem. Phys. 11 (2009) 9188.

[8] D. Fernández-Torre, K. Kosmider, J. Carrasco, M. V. Ganduglia-Pirovano, R. Pérez, J. Phys. Chem. C 116 (2012) 13584.

[9] Y. G. Wang, D. Mei, J. Li, R. Rousseau. J. Phys. Chem. C 117 (2013) 23082.

[10] F. Esch, S. Fabris, L. Zhou, T. Montini, C. Africh, P. Fornasiero, G. Comelli, R. Rosei . Science 309 (2005) 752.

[11] J. L. F. Da Silva, M. V. Ganduglia-Pirovano, J. Sauer, V. Bayer, G. Kresse, Phys. Rev. B 75 (2007) 045121.

[12] Y. M. Choi, H. Abernathy, H.-T. Chen, M. C. Lin, M. Liu. ChemPhysChem 7 (2006) 1957.

[13] M. Huang, S. Fabris. Phys. Rev. B 75 (2007) 081404 (R).

[14] M. Nolan. J. Phys. Chem. C 115 (2011) 6671.

[15] S. M. Kozlov, F. Viñes, N. Nilius, Sh. Shaikhutdinov, K. M. Neyman. J. Phys. Chem. Lett. 3 (2012) 1956.

[16] R. Farra, M. García-Melchor, M. Eichelbaum, M. Hashagen, W. Frandsen, J. Allan, F. Girgsdies, L. Szentmikloski, N. López, D. Teschner. ACS Catal. 3 (2013) 2256.

[17] G. Vilé, S. Colussi, F. Krumeich, A. Trovarelli, J. Pérez-Ramírez. Angew. Chem. Int. Ed. 53 (2014) 12069.

[18] M. García-Melchor, N. López. J. Phys. Chem. C 118 (2014) 10921.

[19] J. Carrasco, G. Vilé, D. Fernández-Torre, R. Pérez, J. Pérez-Ramírez, M. V. Ganduglia-Pirovano. J. Phys. Chem. C 118 (2014) 5352.

[20] F. R. Negreiros, S. Fabris. J. Phys. Chem. C 118 (2014) 21014.

[21] S. Fabris, S. de Gironcoli, S. Baroni, G. Vicario, G. Balducci. Phys. Rev. B 71 (2005) 041102(R).

[22] V. I. Anisimov, J. Zaanen, O. K. Andersen. Phys. Rev. B 44 (1991) 943.

[23] V. I. Anisimov, I. V. Solovyev, M. A. Korotin, M. T. Czyzyk, G. A. Sawatzky. Phys. Rev. B 48 (1993) 16929.

[24] S. Fabris, G. Vicario, G. Balducci, S. de Gironcoli, S. Baroni. J. Phys. Chem. B 109 (2005) 22860.

[25] C. Loschen, J. Carrasco, K. M. Neyman, F. Illas, Phys. Rev. B 75 (2007) 035115.

[26] A. Iwaszuk, M. Nolan. J. Phys. Chem. C 115 (2011) 12995.

[27] L. J. Bennet, G. Jones. Phys. Chem. Chem. Phys. 16 (2014) 21032.

[28] M. Cococcioni, S. de Gironcoli, Phys. Rev. B 71 (2005) 035105.

[29] F. Zhou, M. Cococcioni, C. A. Marianetti, D. Morgan, G. Ceder, Phys. Rev. B 70 (2004) 235121.

[30] H. J. Kulik, M. Cococcioni, D. A. Scherlis, N. Marzari, Phys. Rev. Lett. 97 (2006) 103001.

[31] M. T. Curnan, J. R. Kitchin. J. Phys. Chem. C 118 (2014) 28776.

[32] B. Meredig, A. Thompson, H. A. Hansen, C. Wolverton. Phys. Rev. B 82 (2010) 195128.

[33] J. J. Plata, A. M. Márquez, J. Fdez. Sanz. J. Chem. Phys. 136 (2012) 041101.

[34] S. Carrettin, P. Concepcion, A. Corma, J. M. Lopez-Nieto, V. F. Puntes. Angew. Chem., Int. Ed. 43 (2004) 2538.

[35] J. Guzman, S. Carrettin, A. Corma, J. Am. Chem. Soc. 127 (2005) 3286.

[36] Z. Wu, M. Li, S. H. Overbury. J. Catal. 285 (2012) 61.

[37] J. Xu, J. Harmer, G. Li, T. Chapman, P. Collier, S. Longworth, S. C. Tsang. Chem. Commun. 46 (2010) 1887.

[38] C. Loschen, S. T. Bromley, K. M. Neyman, F. Illas. J. Phys. Chem. C Lett. 111 (2007) 10142.

[39] C. Loschen, A. Migani, S. T. Bromley, F. Illas, K. M. Neyman. Phys. Chem. Chem. Phys. 10 (2008) 5730.

[40] A. Migani, G. M. Vayssilov, S. T. Bromley, F. Illas, K. M. Neyman, Chem. Commun. 46 (2010) 5936.

[41] G. N. Vayssilov, M. Mihaylov, P. St. Petkov, K. Hadjiivanov, K. M. Neyman. J. Phys. Chem. C. 115 (2011) 23435.

[42] G. Preda, A. Migani, K. M. Neyman, S. T. Bromley, F. Illas, G. Pacchioni. J. Phys. Chem. C 115 (2011) 5817.

[43] J. P. Perdew, J. A. Chevary, S. H. Vosko, K. A. Jackson, M. R. Pederson, D. J. Singh, C. Fiolhais. Phys. Rev. B 46 (1992) 6671.

[44] J. P. Perdew, Y. Wang. Phys. Rev. B 45 (1992) 13244.

[45] G. Kresse, J. Furthmüller. Phys. Rev. B 54 (1996) 11169.

[46] G. Kresse, J. Hafner. Phys. Rev. B 47 (1993) 558.

[47] P. E. Blöchl. Phys. Rev. B 50 (1994) 17953.

[48] E. Sanville, S. D. Kenny, R. Smith, G. Henkelman. J. Comput. Chem. 28 (2007) 899.

[49] G. Henkelman, A. Arnaldsson, H. Jonsson. Comput. Mater. Sci. 36 (2006) 354.

[50] S. L. Dudarev, G. A. Botton, S. Y. Savrasov, C. J. Humphreys, A. P. Sutton. Phys. Rev. B 57 (1998) 1505.

[51] C. Li, K. Domen, K. Mayura, T. Onischi. J. Catal. 123 (1990) 436.

[52] A. Martínez-Arias, J. Conesa, J. Soria. Res. Chem. Intermed. 33 (2007) 775.